Supplementary Information to: "Low electron-polar optical phonon scattering at the fundament of high carrier mobility in methylammonium lead-iodide perovskites."

A. Filippetti[1], A. Mattoni[1], C. Caddeo[1], M. I. Saba[1], and P. Delugas[2]

[1]Istituto Officina dei Materiali, CNR-IOM SLACS Cagliari, Cittadella Universitaria, Monserrato 09042-I (CA), Italy.

[2] Scuola Internazionale di Studi Superiori Avanzati - Via Bonomea 265, 34136 - Trieste, Italy.

1. Relaxation time: quantum mechanical modeling

For our electronic transport calculations we used model expressions for the scattering relaxation time, dependent on carrier energy and temperature. These expressions are derived from a quantum mechanical treatment with some suited approximations, namely parabolic band behavior (but including anisotropic masses) for the electronic band structure and simple parameterizations for the phonon bands (linear dispersion for acoustic phonons, fixed energies for polar optical phonons). We included three scattering processes: impurity scattering (IS), acoustic phonon scattering (APS), and polar optical

phonon scattering (POS). The total scattering rate is thus obtained according to the Matthiessen's rule, as:

$$\tau_{rel}^{-1}(T,\varepsilon) = \tau_{IS}^{-1}(T,\varepsilon) + \tau_{APS}^{-1}(T,\varepsilon) + \tau_{POS}^{-1}(T,\varepsilon) \qquad (1)$$

In the following, we first derive the general quantum mechanical expression for the relaxation time in case of elastic scattering, and then the specific formulas for the three processes mentioned above. Finally, we describe our calculation for the deformation potentials of MAPI, which is a key parameter for the modeling, and at our knowledge not yet reported in literature.

1.1 General expression for elastic scattering

Bloch-Boltzmann transport starts from the assumption that the mean free path of the electron is much larger than the characteristic electron wavelength. In this hypothesis, even in presence of scattering (out of equilibrium) the crystalline momentum can be still assumed as good quantum number and the electron still occupies a Bloch state $|n\mathbf{k}\rangle$; the action of scattering is thus moving the carrier from $|n\mathbf{k}\rangle$ to $|n\mathbf{k'}\rangle$ (assuming intra-band scattering only). The change of distribution function due to collisions is:

$$\left.\frac{\partial f(k)}{\partial t}\right|_{col} = -\int dk' \{W(k \to k')f(k)[1-f(k')] - W(k' \to k)f(k')[1-f(k)]\} \quad (2)$$

where the 2 terms are for scattering into or out of k, W the scattering rate, and Pauli principle has been accounted. At equilibrium the net collision rate vanishes (principle of detailed balance):

$$W(k \to k')f_0(k)[1-f_0(k')] - W(k' \to k)f_0(k')[1-f_0(k)] = 0 \quad (3)$$

Also the Boltzmann distribution can be written, to the linear order in the electric field:

$$f(k) = f_0(k) - \varphi(k)\frac{\partial f_0}{\partial \varepsilon_k}; \qquad\qquad \varphi(k) = \pm |e| \tau \mathbf{E} \cdot \mathbf{v}_g \quad (4)$$

After substitution of Eq.3 and 4 in Eq.2 and some manipulations, it can be shown that the collision rate in case of elastic scattering can be expressed through the definition of an energy-dependent relaxation time:[1]

$$\left.\frac{\partial f(k)}{\partial t}\right|_{col} = -\frac{(f(k) - f_0(k))}{\tau} \qquad (5)$$

where:

$$\tau^{-1}(\varepsilon_k) = \sqrt{\frac{m_x^* m_y^* m_z^*}{m_e^3}} \int d\mathbf{k}' \mathrm{W}(\mathbf{k}, \mathbf{k}')(1 - \cos \vartheta_{kk'}) \qquad (6)$$

1.2 Impurity scattering.

Following the Brooks-Herring development (in 3D), the probability that the electron undergoes a momentum change from $\mathbf{k}$ to $\mathbf{k}'$ due to the scattering with the Coulomb potential of a ionized impurity with ionic charge Z_I and concentration n_I is:

$$\mathrm{W}(\mathbf{k}, \mathbf{k}') = \frac{n_I}{4\pi^2 \hbar}\left[\frac{Z_I e^2}{\varepsilon_0 \left(|\mathbf{k} - \mathbf{k}'|^2 + \mathbf{q}_0^2\right)}\right]^2 \delta(\varepsilon_{n\mathbf{k}} - \varepsilon_{n\mathbf{k}'}) \qquad (7)$$

Clearly the delta function expresses the energy conservation; ε_0 is the dielectric constant, and $q_0^2 = e^2 n_I /(\varepsilon_0 K_B T)$ the squared Debye screening length. Substituting Eq.7 into Eq.6 and solving the integral assuming parabolic band modeling, we obtain the well-known Brooks-Herring formula:

$$\tau_{IS}^{-1}(T, \varepsilon) = \frac{\pi n_I Z_I^2 \varepsilon^{-3/2}}{\sqrt{2\tilde{m}}}\left(\frac{e^2}{4\pi\varepsilon_0}\right)^2 \left[\log\left(1 + \frac{8\tilde{m}\varepsilon}{\hbar^2 q_0^2}\right) - \frac{1}{1 + \left(\hbar^2 q_0^2 / 8\tilde{m}\varepsilon\right)}\right] \qquad (8)$$

where $\tilde{m} = \left(m_x^* m_y^* m_z^*\right)^{1/3}$ is the geometrically averaged band mass.

1.3 Acoustic phonon scattering.

Strictly speaking, the scattering with acoustic phonons is an inelastic process; however, since acoustic phonon energies are typically small, we can still use Eq.6 to define a relaxation time. From the Fermi golden rule:

$$W(\mathbf{k}N,\mathbf{k'N'}) = \frac{2\pi}{\hbar}\left[\langle\mathbf{k'}N'|H_{int}|\mathbf{k}N\rangle\right]^2 \delta\left(E_{\mathbf{k'},N'} - E_{\mathbf{k},N}\right) \qquad (9)$$

where $\mathbf{k}, N$ and $\mathbf{k'}, N'$ are electron momentum and phonon occupancy of initial and final states, respectively. We can model the long-wavelength limit of the acoustic waves as an homogeneous strain:

$$H_{int}(\mathbf{r}) = \sum_i \frac{\partial \varepsilon_{k_0}}{\partial \eta_i} \eta_i(\mathbf{r}) \qquad (10)$$

where the linear change of the band edge with an applied strain is called *deformation potential D*:

$$D_i = \frac{\partial \varepsilon_{k_0}}{\partial \eta_i} \qquad (11)$$

where *i=x, y, z*, and the strain can be expressed as the linear-order derivative of the space dilatation:

$$\eta_i(\mathbf{r}) = \frac{\partial u_i(\mathbf{r})}{\partial \mathbf{r}_i} \qquad (12)$$

Then, substituting Eqs.10-12 into Eq.9 and Eq.6, and assuming parabolic band modeling and linear acoustic phonon dispersion, it can be shown[1] that the relaxation time for the acoustic phonon scattering in the deformation potential approximation is:

$$\tau_{AP}^{-1}(T,\varepsilon) = \frac{(2\tilde{m})^{3/2} K_B T D^2 \varepsilon^{1/2}}{2\pi\hbar^4 \rho v_s^2} + \frac{e^2 (2\tilde{m})^{1/2} K_B T \zeta^2 \varepsilon^{-1/2}}{4\pi\varepsilon_0 \hbar^2} \qquad (13)$$

where ρ is the mass density, v_s the sound velocity, $\tilde{m}$ the geometrically averaged band mass. Emission and absorption contributions are both included in Eq.13. The 2nd term to the right is the piezoelectric scattering, i.e. the contribution due to the change in polarization induced by an elastic strain in case of polar materials; ζ is an adimensional parameter called electromechanical coupling.

1.4 Polar optical phonon scattering.

The scattering with optical phonons is essentially inelastic, thus the simple expression of Eq.6 cannot be applied. Nevertheless, it was shown by Ridley[2,3] that an appropriate generalization to the relaxation time can still be furnished. However, the exact treatment is too cumbersome to be used in practical calculations, thus we recur to an approximation which is still sufficiently accurate for our means. Following Ridley, for a relevant longitudinal optical phonon of energy $\hbar\omega_{LO}$ we take:

$$\tau_{POS}(T,\varepsilon) = \frac{Z\varepsilon^{3/2}}{C(T,\varepsilon)} \qquad\qquad \varepsilon < \hbar\omega_{LO} \qquad (14)$$

$$\tau_{POS}(T,\varepsilon) = \frac{Z\varepsilon^{3/2}}{C(T,\varepsilon) - A(T,\varepsilon) - B(T,\varepsilon)} \qquad \varepsilon > \hbar\omega_{LO} \qquad (15)$$

where:

$$A(T,\varepsilon) = \left(N(\hbar\omega_{LO}) + 1\right)\frac{f(\varepsilon + \hbar\omega_{LO})}{f(\varepsilon)} \times$$

$$\times \left\{ (2\varepsilon + \hbar\omega_{LO})\sinh^{-1}\left(\frac{\varepsilon}{\hbar\omega_{LO}}\right)^{1/2} - [\varepsilon(\varepsilon + \hbar\omega_{LO})]^{1/2} \right\} \qquad (16)$$

$$B(T,\varepsilon)=\theta\left(\varepsilon-\hbar\omega_{LO}\right)N(\hbar\omega_{LO})\frac{f(\varepsilon-\hbar\omega_{LO})}{f(\varepsilon)}\times$$

$$\times\left\{(2\varepsilon-\hbar\omega_{LO})\cosh^{-1}\left(\frac{\varepsilon}{\hbar\omega_{LO}}\right)^{1/2}-\left[\varepsilon(\varepsilon-\hbar\omega_{LO})\right]^{1/2}\right\} \tag{17}$$

$$C(T,\varepsilon)=2\varepsilon\left(N(\hbar\omega_{LO})+1\right)\frac{f(\varepsilon+\hbar\omega_{LO})}{f(\varepsilon)}\sinh^{-1}\left(\frac{\varepsilon}{\hbar\omega_{LO}}\right)^{1/2}+$$

$$+2\varepsilon\,\theta\left(\varepsilon-\hbar\omega_{LO}\right)N(\hbar\omega_{LO})\cosh^{-1}\left(\frac{\varepsilon}{\hbar\omega_{LO}}\right)^{1/2} \tag{18}$$

$$Z^{-1}=\omega_{LO}\frac{e^2}{4\pi\hbar^2}\left(\frac{m^*}{2}\right)^{1/2}\left(\frac{1}{\varepsilon_\infty}-\frac{1}{\varepsilon_0}\right) \tag{19}$$

Eq.14 is quite accurate for $\varepsilon<\hbar\omega_{LO}$, while Eq.15 is exact in the $\varepsilon\gg\hbar\omega_{LO}$ limit, and a reasonable approximation for $\varepsilon>\hbar\omega_{LO}$. When more than a single LO phonon is important for the scattering processes, they can be treated as independent scatterers and then summed according to Matthiessen's rule.

1.5 Parameters.

The parameters entering the relaxation time expressions for MAPI are in large portion well established in literature: $v_s=3.1\mathrm{x}10^5$ cm/s, $\varepsilon_0=60$ (at room-T), $\varepsilon_\infty=6.5$, $\tilde{m}\approx0.2m_e$, $\hbar\omega_{LO}=80.9$ cm^{-1}. Also, we take $\zeta=0$, since at room-T (which is the temperature region of more interest for our means) the piezoelectric response of MAPI can be assumed small or discardable. On the other hand, at our knowledge, an evaluation of the deformation potentials in literature was missing, thus we performed accurate calculations to establish the values of D for electrons and holes in the orthorhombic structure.

2. Deformation potentials of MAPI.

We calculated the deformation potentials for MAPI by finite differences, i.e. applying ±1% strains along the three axes of the orthorhombic structures, and evaluating the changes induced at the band extremes. The band structure results are reported in Fig.S1. In the calculations under strain the atoms are kept fixed to their ground-state crystal coordinates, in order to include only the change due to a pure space dilatation or contraction. Also, the spurious rigid-shift effects on the band structure due to electrostatic potential change under strain has been extracted out in Fig.S1 by careful realignment of the deepest Pb (5d) semi-core levels.
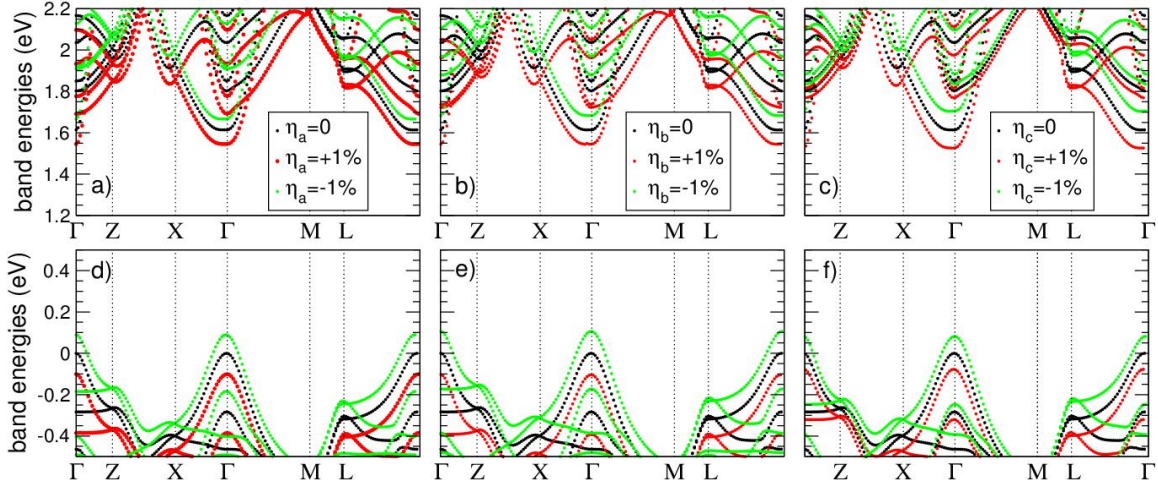
Figure S1: Band structure of orthorhombic MAPI in the equilibrium structure (black lines) and under an applied positive (red lines) and negative (green lines) strain of 1%. Panels a), b), c) display conduction bands for strains applied along the *a*, *b*, *c* axes of the orthorhombic cell, respectively; panels d), e), f) are for strains applied along *a*, *b*, *c* but for valence bands.

The valence band top and conduction band bottoms at Γ point calculated for the orthorhombic ground-state structure (described in Ref.4) and the structure under positive and negative 1% strain, are reported in Tab.S1. The ground-state VBT is fixed at zero, thus the CBB equals the band gap. The deformation potential is calculated as the change in the band energy extrema for the applied strain, averaging over positive and negative strains; thus for conduction:

$$D_j = \frac{1}{2\eta}\left\{\left[\varepsilon_{CBB}(\eta=0.01)-\varepsilon_{CBB}(\eta=0)\right]+\left[\varepsilon_{CBB}(\eta=-0.01)-\varepsilon_{CBB}(\eta=0)\right]\right\} \quad (20)$$

for j=a, b, c, and analogous equation for the VBT.

Table S1: Calculated valence (VBT) and conduction (CBB) band extremes for MAPI in the ground-state orthorhombic structure (unstrained) and under applied ±1% strain along the axes of the orthorhombic cell. The deformation potentials D_i average the band shifts for positive and negative strain. D is the deformation potential averaged over the 3 axes. The band gaps for the strains along the three directions are also reported.

	ε_{VBT} (eV)	ε_{CBB} (eV)	E_{gap} (eV)
unstrained	0.0	1.614	1.614
a axis			
$\eta=-1\%$	0.089	1.666	1.577
$\eta=+1\%$	-0.101	1.546	1.647
D_a	-9.5	-6.046	
b axis			
$\eta=-1\%$	0.105	1.683	1.578
$\eta=+1\%$	-0.104	1.545	1.649
D_b	-10.48	-6.88	
c axis			
$\eta=-1\%$	0.082	1.705	1.623
$\eta=+1\%$	-0.077	1.526	1.603
D_c	-7.94	-8.97	
D	-9.31	-7.30	

From Tab.S1 we see that the deformation potentials are always negative, i.e. a positive strain (lattice stretching) shift down both VBT and CBB energies along each direction, while a negative strain (lattice shrinking) shift VBT and CBB to lower energies. This is reasonable, since the anti-bonding Pb (6s, 6p) states are stabilized by an increase of Pb-I distance, and destabilized by a Pb-I shrinking. Notice that the sing of the deformation potential has no effects on the scattering rate with the acoustic phonons, which depends on D^2 (Eq.13). Also, since we are interested in the 3D-averaged transport properties, we considered the 3D-averaged deformation potentials, also reported in the Table: -9.31 eV and -7.30 eV for holes and electrons, respectively, are those used for our transport

calculations described in the article. These values are typical of ordinary semiconductors, e.g. for bulk GaAs the conduction band deformation is reported between -7 and -9.5 eV[5] . This similarity highlights once more the inorganic character of MAPI.

[1] M. Balkanski, and R. F. Wallis. *Semiconductor Physics and Applications*, Oxford University Press, New York, **2000.**

[2] B. K. Ridley, *J. Phys.: Condens. Matter* **1998,** *10*, 6717–6726.

[3] D. R. Anderson, N. A. Zakhleniuk, M. Babiker, B. K. Ridley, and C. R. Bennett, *Phys. Rev B*, **2001**, *63*, 245313.

[4] A. Filippetti and A. Mattoni. Hybrid perovskites for photovoltaics: Insights from first principles. *Phys. Rev. B*, **2014,** *89*, 125203.

[5] X. Zianni, P. N. Butcher, and M. J. Kearney, *Phys. Rev. B* **1994**, *49*, 7520.